Trace element constraints on mid-crustal partial melting processes – A garnet ionprobe study from polyphase migmatites (Damara orogen, Namibia)

C. Jung[1], S. Jung[2,3], E. Hellebrand[2,4] and E. Hoffer[1]

[1] Fachbereich Geowissenschaften, Philipps Universität Marburg, 35032 Marburg, FRG

[2] Max-Planck-Institut für Chemie, Abt. Geochemie, Postfach 3060, 55020 Mainz, FRG

[3] Department Geowissenschaften, Mineralogisch-Petrographisches Institut, Universität Hamburg, 20146 Hamburg, FRG
Email: stefan.jung@mineralogie.uni-hamburg.de

[4] SOEST – Department of Geology and Geophysics, University of Hawaii, USA

ABSTRACT: Trace element abundances in garnet from a polyphase migmatite were measured by secondary ion mass spectrometry (SIMS) in order to identify some of the effective variables on the trace element distribution between garnet and melanosome or leucosome. In general, garnet is zoned with respect to REE, in which garnet cores are enriched by a factor of 2–3 relative to the rims. For an inclusion-rich garnet from the melanosome, equilibrium distribution following a simple Rayleigh fractionation is responsible for the decreasing concentrations in REE from core to rim. Inclusion-poor garnet from the same melanosome located in the vicinity of the leucosomes shows distinct enrichment and depletion patterns for REE from core to rim. These features suggest disequilibrium between garnet and the host rock which, in this case, could have been an *in-situ* derived melt. This would probably indicate a period of open-system behaviour at a time when the garnet, originally nucleated in the metamorphic environment reacted with the melt. In addition, non-gradual variation in trace element abundances between core and rim may suggest variable garnet growth rates. Inclusion-free garnet from the leucosome, interpreted to have crystallised in the presence of a melt, has a small core with high REE abundances and a broad rim with lower REE abundances. Here, crystal-liquid diffusion-controlled partitioning is a likely process to explain the trace element variation.

KEY WORDS: *in situ* partial melting, granites, migmatites, trace element composition

Garnet is the major mineral used for the reconstruction of P–T paths because it is involved in a number of reactions useful for thermobarometry (e.g. Essene 1989). Consequently, the major element zoning of garnet has been widely used to investigate the P–T conditions of regional metamorphic terranes (Tracy 1982; Spear & Selverstone 1983; Spear *et al*. 1984). The chemical signatures of the early stages of regional metamorphism are often preserved up to the lower amphibolite facies, due to the slow diffusivities of the major cations Fe, Mg, Mn and Ca. However, prograde chemical zoning is rare in high-grade garnet of amphibolite- to granulite-facies terranes, due to enhanced intracrystalline diffusion at higher temperatures (Spear & Florence 1992). On the other hand, it has been demonstrated that trace element zoning in garnet is often more pronounced than major element zoning (Hickmott *et al*. 1987; Hickmott & Shimizu 1990; Hickmott & Spear 1992; Spear & Kohn 1996; Chernoff & Carlson 1999; Otamendi *et al*. 2002). This implies that trace elements may potentially be less sensitive to chemical changes in rocks than major elements. Accurate interpretation of major and trace element zoning in garnet can therefore lead to significantly improved understanding of the evolutionary path of metamorphism and hence of the tectonic evolution of mountain belts.

Prograde heating of crustal segments will ultimately result in fluid-absent partial melting of metasedimentary rocks, producing a granitic melt and an aluminous residue in which the restitic mineral assemblage will control the trace element concentration of the melt. The mineralogical composition of the residual assemblage is dependent on the nature of the melting reaction and the pressure at which melting occurs. Garnet is a common refractory mineral phase that may be present in the high-grade metasedimentary protolith, or a product of incongruent melting reactions at higher metamorphic grade. A detailed knowledge of the distribution of trace elements between garnet, metamorphic host rock or melt is therefore critical for trace element modelling of anatectic crustal melts. In order to identify some of the effective variables on the trace element distribution between garnet and the host rock, this study presents trace element data on garnet measured by SIMS from a polyphase migmatite terrane from the Damara orogen (Namibia). It is shown that trace element variation during garnet growth during regional metamorphism and melting provides additional constraints on the garnet-forming process with important implications for the geochemical signature of granitic melts.

 doi:10.1017/S1755691009016107

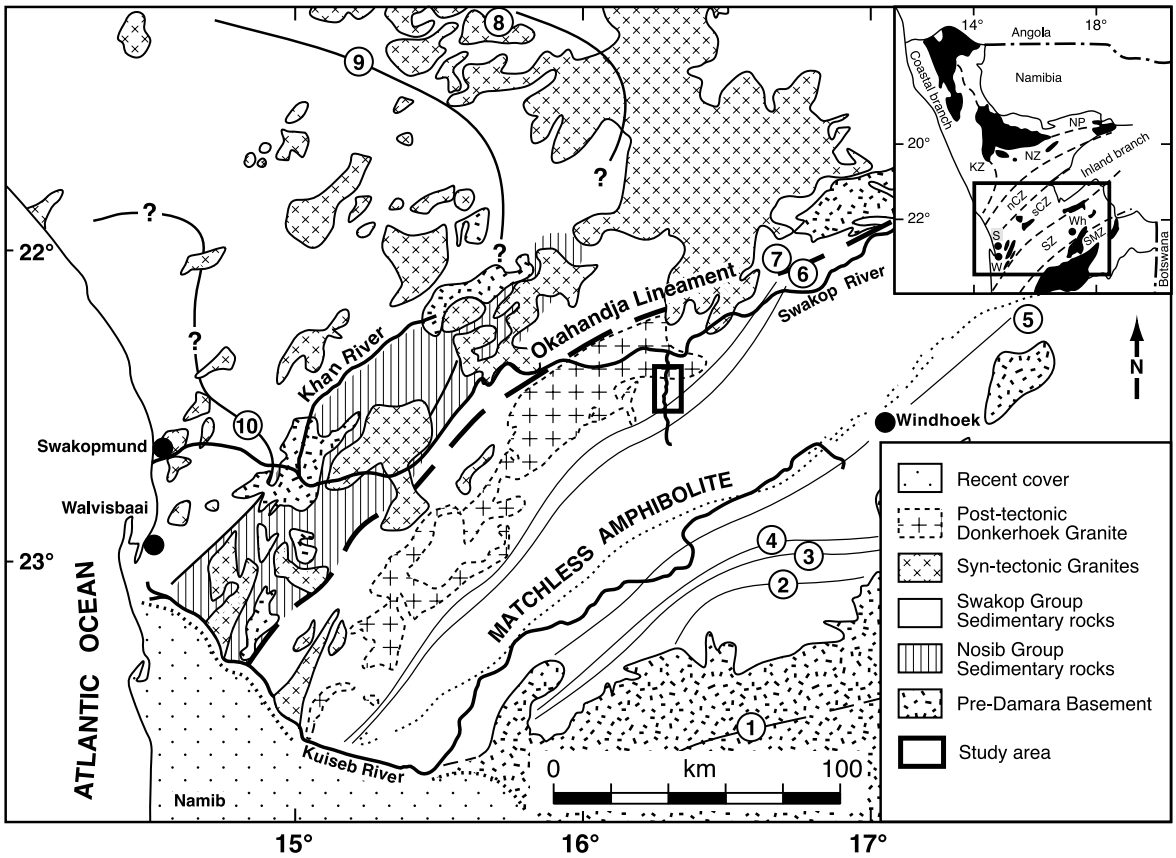

Figure 1 Generalised geological map showing the study area within the transition zone between the lower part of the southern Central Zone and Southern Zone of the Damara orogen, Namibia. Abbreviations in inset: KZ=Kaoko Zone; NP=Northern Platform; NZ=Northern Zone; nCZ=northern central Zone; sCZ=southern Central Zone; SZ=Southern Zone; SMZ=Southern Margin Zone. Isograd map (Hartmann *et al.* 1983) gives the distribution of pan-African regional metamorphic isograds within the southern and central Damara orogen. Isograds: (1) biotite-in; (2) garnet-in; (3) staurolite-in; (4) kyanite-in; (5) cordierite-in; (6) andalusite <--->sillimanite; (7) sillimanite-in according to staurolite-breakdown; (8) partial melting due to: muscovite+plagioclase+quartz+H_2O <--->melt+sillimanite; (9) K-feldspar+cordierite-in; (10) partial melting due to: biotite +K-feldspar+plagioclase+quartz+cordierite <--->melt+garnet.

1. Geological setting

The Damara orogen of Namibia comprises a deeply eroded section of a Pan-African mobile belt that can be divided into a N–S-trending coastal branch, the Kaoko belt, and a NE–SW-trending intracontinental branch (see inset to Fig. 1). This mobile belt has been divided into several zones based mainly on stratigraphy, metamorphic grade, structure and geochronology (Miller 1983). The intrusive rocks record ages between 750 Ma and 480 Ma and crop out over an area of approximately 75 000 km^2 (Fig.1). Granites are the most common igneous rock type (c. 94%) and the remaining intrusions are equally divided between diorite and tonalite/granodiorite (Miller 1983). Pre-Damara basement gneisses are overlain by various metasedimentary sequences containing quartzose sandstones, arkoses, schists and calc-silicate rocks, marble, conglomerate, metamorphosed glaciogenic diamictites, banded iron-stones, Al-rich metapelite and carbonates.

In the Central Zone (Fig. 1), the metamorphic grade increases from east to west, reaching high-grade conditions with local partial melting in the coastal area (Hartmann *et al.* 1983). Early maximum estimates for the peak metamorphic temperatures were ca. 645°C at 3 ± 1 kbar obtained on impure marbles (Puhan 1983) and ca. 650°C based on oxygen isotope fractionation in a variety of metasedimentary and metaigneous rocks (Hoernes & Hoffer 1979). More recently, pressure–temperature estimates were substantially revised indicating low-pressure high-temperature granulite facies conditions with temperatures between 700–750°C at 5–6 kbar (Masberg *et al.* 1992; Jung & Mezger 2003; Ward *et al.* 2008). These new p–t estimates are generally considered to be too low to cause widespread biotite dehydration melting, however, migmatisation is a local phenomenon and is not accompanied by large volumes of newly-formed melt. There is some disagreement as to whether the initial steps of melting were caused by muscovite-dehydration melting, since metamorphic K-feldspar is a common mineral in high-grade metapelites (Jung *et al.* 1999; Jung & Mezger 2003). On the other hand, initial partial melting under water-saturated conditions is a possibility; in this case the water may have come from some of the plutons associated with the migmatites. One major step forward in the interpretation of the metamorphic history of the Damara orogen is provided by Ward *et al.* (2008), who showed that fluid-assisted partial melting involving biotite breakdown is a possibility to explain some of the migmatites in the central Damara orogen. The large amount of sizeable plutons observed in the Central Damara orogen originated by partial melting processes in the deeper crust where temperatures in excess of 800–850°C are not unlikely.

To the south-east, there is a gradation into the Okahandja Lineament Zone that separates the Central Zone from the Southern Zone (Fig. 1). In the Southern Zone, regional metamorphism is characterised by a Barrovian-type sequence, with a general increase in the metamorphic grade from south to north. The metamorphic conditions range from low to medium pressures and reached up to 8 kbar at maximum temperatures of 600°C. There is evidence that suggests that

https://doi.org/10.1017/S1755691009016107 Published online by Cambridge University Press

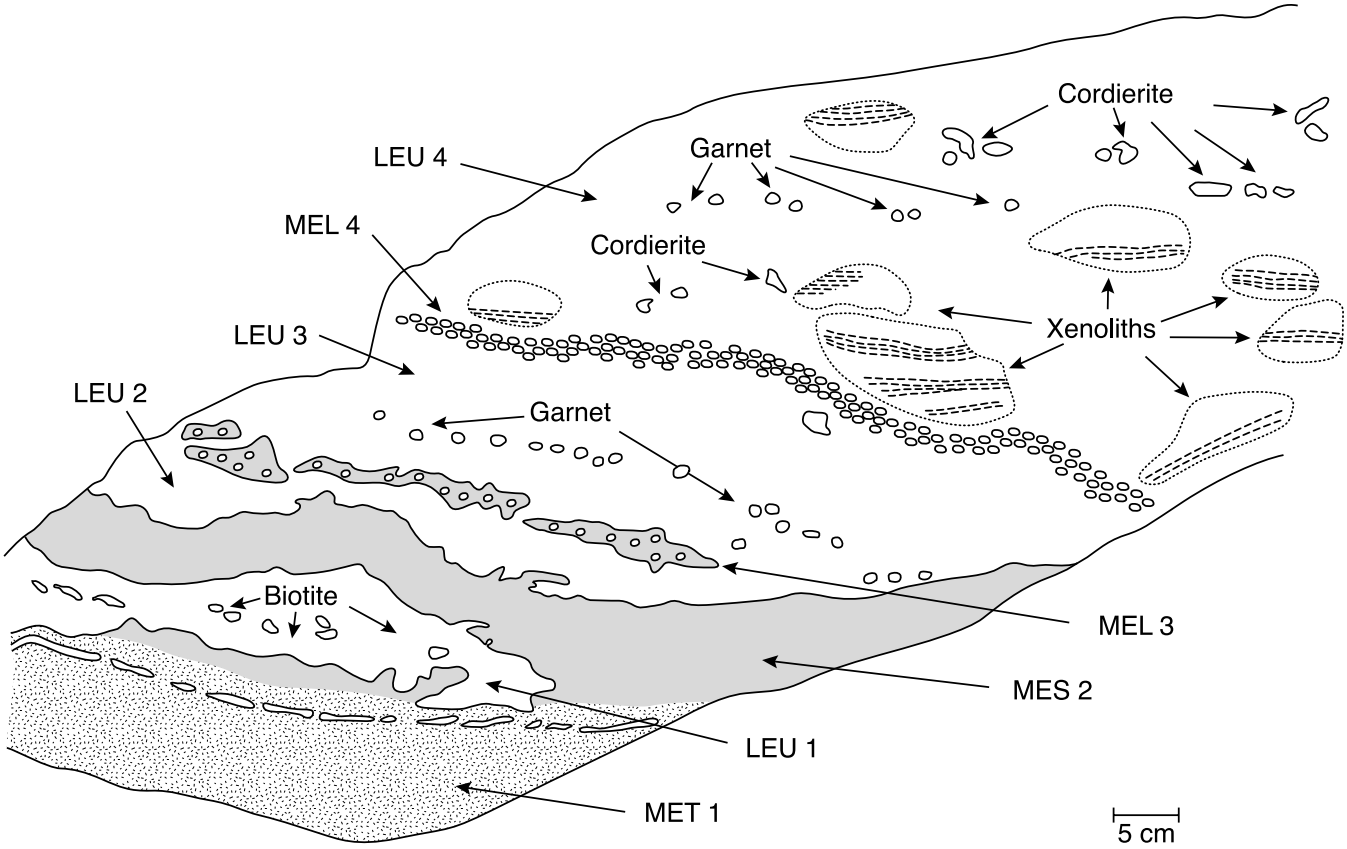

Figure 2 Sketch of the migmatite sample from the Davetsaub area showing the different lithological units.

regional metamorphism in the Southern Zone is more or less coeval with regional metamorphism in the Central Zone. This interpretation is based on U–Pb and Pb–Pb garnet and staurolite ages of 550 ± 10 Ma and 480 ± 20 Ma (Jung 2005), similar to the range of U–Pb monazite and Sm–Nd garnet ages obtained from metapelites and migmatites from the Central Zone. U–Pb garnet and staurolite ages must be interpreted with caution, since any incorporated high-U/Pb microinclusion may totally cover the initial radiogenic isotope composition of garnet and staurolite. However, in the present case, $^{206}Pb/^{204}Pb$ ratios of garnet and staurolite are <50, suggesting that high U/Pb inclusions do not play a major role here and the ages, although associated with a relatively large error, date the time of garnet and staurolite growth.

Rb–Sr and K–Ar biotite ages indicate cooling to 350–300 °C between 480 Ma and 460 Ma (Miller 1983). More recently, Gray *et al*. (2006) obtained Ar–Ar isotope data on white mica and biotite, indicating cooling to 300–350 °C between 495 Ma and 480 Ma. Intrusion of large volumes of granitic rocks are absent even in the highest grade zone of the Southern Damara orogen.

The formation of the migmatites of Davetsaub and Nomatsaus (22·4 °S/16·3 °E, Fig. 1) was originally thought to be related to the intrusion of the peak-metamorphic post-deformational Donkerhoek granodiorite (Nieberding 1976; Saywer 1981). Since the granodiorite has no extensive thermal aureole, the country rocks are assumed to have been still hot at the time of emplacement. Based on the geological map (Miller 1983), isotopic investigations by Kukla (1993), and detailed field investigations by the present authors, it is more likely that the Davetsaub area represents a portion of the Damaran metasedimentary rocks where intrusion of older granites produced various types of migmatites. Kukla (1993) presented structural evidence that the anatectic event that generated the migmatites occurred relatively late within the deformational history of the Damara orogen, but clearly predates the intrusion of the Donkerhoek granodiorite.

2. Description of the migmatite

Macroscopic and mesoscopic descriptions of the migmatites from the Davetsaub and Nomatsaus areas have been published by Kukla (1993), Kukla *et al*. (1991) and Jung *et al*. (1998). Additional information about the mineralogical composition of the different sub-domains of the migmatite (mesosome, melanosome, leucosome) is given in Jung *et al*. (1998). Metasedimentary and migmatitic rocks outcropping at the Davetsaub and Nomatsaus areas (Fig. 1) are fine to medium-grained dark-grey to dark-brown pelitic gneisses with a fabric defined by alternating biotite-bearing and biotite-poor domains. Most pelitic gneisses are impregnated by pegmatitic material, as well as concordant to discordant leucosomes. Banded migmatites are commonly folded, and most of the pegmatites cut the main foliation. Mesosomes (nomenclature according to Brown 1983) and leucosomes are well segregated and locally separated by biotite–garnet–cordierite-bearing melanosomes. Some leucocratic layers contain isolated xenoliths with the mineral assemblage quartz + plagioclase + sillimanite ± garnet ± K-feldspar ± biotite (Fig. 2). In some areas, the proportion of leucocratic material dominates, so that some melanosomes appear as rafts surrounded by leucosome material and the resulting rock is a diatexite. In the biotite-bearing domains of the mesosomes and melanosomes, the fabric is defined by aligned biotite flakes, biotite–sillimanite intergrowths, xenomorphic garnet porphyroblasts with inclusions of biotite, sillimanite, plagioclase and spinel and poikilitic, elongated, partly pinitised cordierite porphyroblasts with inclusions of sillimanite. Garnet has abundant (<30 μm) inclusions of zircon and monazite. In the biotite-poor domains of

https://doi.org/10.1017/S1755691009016107 Published online by Cambridge University Press

some mesosomes, ribboned quartz aggregates and relict plagioclase porphyroblasts dominate the fabric.

Textural relations preserved within the pelitic migmatites suggest that the assemblage quartz+plagioclase+biotite+cordierite$_{(I)}$+sillimanite was developed at an early stage in the metamorphic history. Subsequently, the growth of garnet ± spinel at the expense of biotite and/or cordierite can be observed. Potential coexistence of spinel and quartz could be interpreted to be indicative of T>800°C during an earlier portion of the metamorphic path, although the significant gahnite component in the spinel suggests stability with quartz could have been possible at slightly lower temperatures (Vielzeuf 1983). There is no petrographic evidence for the coexistence of spinel and quartz, judging from the occurrence of spinel exclusively in garnet and, therefore, high grade metamorphism and partial melting must have occurred prior to the formation of the observed mineral assemblage, when aH_2O was higher. Melting could have been initiated at ca. 670°C at 3–5 kbar, producing small amounts of liquid while efficiently purging the remaining rock of H_2O (Thompson 1982). This initial melting step could have been water-saturated, in which the water needed for H_2O-saturated melting was derived from the nearby plutons. It is, however, difficult or even impossible to prove whether initial melting was water-saturated in rocks that have evolved to higher temperatures, and especially in those rocks that have lost melt. Unfortunately, no precise radiometric age determinations from all plutons in this area are available. In some layers, relict garnet porphyroblasts are often rimmed and partly replaced by coronas of cordierite$_{(II)}$ suggesting decompression later in the metamorphic history.

Garnet in the leucocratic layers of the migmatites is idioblastic and inclusion-free and remained apparently unreacted, or is only locally replaced by an aggregate consisting of green biotite and Ab-rich plagioclase. Fresh cordierite, sometimes twinned, occurs as large sub-idiomorphic grains, with rare inclusions of sillimanite. Minor amounts of late muscovite occur within the leucocratic layers, but not in the metapelitic domains. No prograde andalusite, staurolite or muscovite has been found in the pelitic migmatites and, interestingly no K-feldspar has been found in the residual portions of the migmatites. The high proportion of sillimanite and cordierite/garnet, the fact that metamorphic conditions probably exceed the stability of muscovite plus quartz, and the lack of K-feldspar in the most residual melanosomes suggests that a melt phase coexisted with the melanosomes. This melt phase was subsequently extracted and probably mixed with the leucosomes, since some of these leucosomes are clearly intrusive from the nearby plutons. The lack of K-feldspar and the decreasing abundance of plagioclase and quartz among the mesosomes and melanosomes (see table 1 in Jung *et al*. 1998) is also compatible with the view that a melt phase was extracted. Some of the plagioclase and K-feldspar may have formed cumulates in the leucosomes, since these leucosomes have small but discernable positive Eu anomalies. However, due to the absence of cumulate textures, the limited extraction distances of the leucosomes (some are only centimetres away from the melanosomes), the gradual nature of some leucosome-melanosome pairs and the evidence of progressive entrainment of xenoliths or wall rock material rather then fractional crystallisation, it is suggested that a cumulus nature of the leucosomes is, at least in part, unlikely. In addition, the amount of K-feldspar and plagioclase is way too large to be solely related to the inferred amount of these minerals in the melanosomes and consequently, most of the K-feldspar and plagioclase must be attributed to the original composition of the leucosomes. Note that a complex contamination–accumulation modelling was performed to explain the composition of some of the larger leucosomes associated with the most residual melanosomes (Jung *et al*. 1998) and up to 10 wt.% of K-feldspar/plagioclase may be regarded as accumulated minerals.

It is suggested that consumption of early muscovite+quartz+plagioclase+H_2O led to the formation of a first melt, but the appearance of spinel, garnet and cordierite indicates that also a biotite-dehydration melting reaction was operative. It is therefore reasonable to assume that melt production and extraction probably occurred episodically, both at the maximum P–T conditions and during decompression of the rocks. In summary, petrographic evidence, and thermobarometric constraints, indicate that the migmatites outcropping at the Davetsaub and Nomatsaus areas experienced upper amphibolite to lower granulite facies conditions with temperatures approaching 720–750°C at 4–6 kbars (Saywer 1981; Kukla *et al*. 1991; Jung *et al*. 1998). The major and trace element abundances as well as the Nd, Sr and oxygen isotope compositions suggest that mesosome MES 2, and the melanosomes MEL 3 and MEL 4 (Fig. 2) are strongly residual rocks. The chemical and isotopic composition of the leucosomes can be best explained by a complex partial melting–mixing–accumulation process (Jung *et al*. 1998).

3. Geochronology of the migmatite

Early age determinations on the migmatites from the Davetsaub area yielded a Rb–Sr whole-rock isochron age of 505 ± 5 Ma (Blaxland *et al*. 1979; Haack *et al*. 1982) consistent with a monazite age of 505 ± 4 Ma given by Kukla *et al*. (1991) for the intrusion of a late-tectonic granite in this area. Rb–Sr whole rock ages are 523 ± 8 Ma and 521 ± 15 Ma for the Donkerhoek granite in this area (Blaxland *et al*. 1979). U–Pb monazite ages from the migmatites give ages between 525 ± 2 Ma and 521 ± 2 Ma for composite migmatites and between 521 ± 2 Ma and 518 ± 2 Ma for monazite from neosomes (Kukla *et al*. 1991) providing a lower limit for the peak of metamorphism. More recently, the time of high-grade regional metamorphism and the duration of regional metamorphic events were constrained by Sm–Nd (garnet), U–Pb (monazite) and Rb–Sr (biotite) ages obtained from a composite migmatite sample (Jung & Mezger 2001). Sm–Nd garnet whole rock ages for a strongly restitic melanosome and an adjacent intrusive leucosome yield ages of 534 ± 5 Ma, 528 ± 11 Ma and 539 ± 8 Ma. These results provide substantial evidence for pre-500 Ma Pan-African regional metamorphism and melting for this segment of the orogen. Other parts of the migmatite yielded apparently younger Sm–Nd garnet whole rock ages of 488 ± 9 Ma for melanosome and 496 ± 10 Ma, 492 ± 5 Ma and 511 ± 16 Ma for the corresponding leucosomes. Garnet from one xenolith within the leucosomes yielded an age of 497 ± 2 Ma. Monazite from the leucosomes records $^{207}Pb/^{235}U$ ages of between 536 ± 1 Ma and 529 ± 1 Ma, indicating that this monazite represent incorporated residual material from the first melting event. Monazite from the mesosome and the melanosome gives $^{207}Pb/^{235}U$ ages of between 523 ± 1 Ma and 531 ± 1 Ma, broadly similar to the monazite ages from the leucosomes. The apparently unreacted metasedimentary rock MET 1 yielded a $^{207}Pb/^{235}U$ monazite age of 508 ± 2 Ma, which probably indicate another later thermal event. Taken together, these ages indicate that high-grade metamorphism started at c. 535 Ma (or earlier) and was followed by thermal events between c. 520 Ma and c. 490 Ma. Rb–Sr biotite ages from the different layers of the migmatite are c. 488 Ma, 469 Ma and 473 Ma.

https://doi.org/10.1017/S1755691009016107 Published online by Cambridge University Press

These different ages indicate late-stage disturbance of the Rb–Sr isotopic system on the sub-sample scale. Nevertheless, these ages are close to the youngest Sm–Nd garnet ages indicating rapid cooling rates between 13–20°C/Ma and fast uplift of this segment of the crust (Jung & Mezger 2001).

4. Results

4.1. Garnet major element composition

Garnet is predominantly an almandine–pyrope–spessartine solid solution with a minor grossular component. Inclusion-rich garnet from melanosome MEL 3 has the composition $alm_{69}py_{16}sp_{12}gr_3$ and the inclusion-poor garnet from the same melanosome has the composition $alm_{71}py_{11}sp_{16}gr_2$. Inclusion-free garnet from the melanosome has the composition $alm_{70}py_{17}sp_{11}gr_2$. The garnets from the leucosome and the melanosome show rather similar zoning profiles, with flat element distributions over most of the crystal and increasing Fe/Mg at the outermost rim. There is no pronounced zoning with respect to the grossular component. Details are given in Jung *et al.* (1998).

4.2. Garnet trace element composition

Analytical details are summarised in the Appendix (see section 8). Three texturally distinct garnets can be distinguished, an inclusion-rich (Fig. 3a) and inclusion-poor garnet (Fig. 3b) within the melanosome and an apparently inclusion-free garnet within the leucosome (Fig. 3c). The garnets have a 10^{-3}–10^{3} CI-normalised range in REE abundances and steep LREE-depleted and HREE-enriched element patterns (Fig. 4). A negative Eu anomaly of variable magnitude is developed in the garnets.

4.2.1. Inclusion-rich garnet (melanosome). This garnet (Fig. 3a) has a core composition enriched in HREE+Y and a rim composition that is depleted in HREE+Y (Fig. 4a and b). The core–rim variation is gradual, although Yb and Er display some more enriched domains in the garnet core. Furthermore, the zoning is significantly less pronounced for the middle REE (rim/core ~0·6–1·0 for Sm, Eu, Gd), compared to the more compatible heavy REE (rim/core ~0·2–0·5 for Dy–Yb) and Y (rim/core: 0·5). Furthermore, it shows an irregular or flat distribution of Ti, Cr, Zr and Sc over the crystal, but a tendency for enrichment in V (and to lesser extent Na) can be observed towards the rim of the crystal (Table 1). Asymmetric distribution of Zr of the crystal seems to indicate contamination with micro-inclusions of zircon. Sr seems to be slightly enriched in the core relative to the rim, although the concentrations appear to be similar within error. The distribution of Sm follows roughly that for HREE and Y, with a peak around the core region and depletion in Sm towards the rim. On the other hand, Nd shows a broad core region with low concentrations and a rim composition with elevated concentrations (Fig. 4c). Towards the outermost rim, Nd concentrations decrease again. However, fractionation of LREE ($(Sm/Nd)_N$ ratio, where N denotes normalisation to chondrite, according to Boynton 1984) seems to be more or less constant throughout the crystal (Table 1). On the other hand, fractionation of HREE (Yb/Dy and Yb/Er ratios) is more pronounced for the core than for the rim (Fig. 5). The magnitude of the negative Eu anomaly ranges from 0·03 to 0·09 with a tendency to decrease towards the rim.

4.2.2. Inclusion-poor garnet (melanosome). This garnet has also a core composition enriched in HREE+Y and a rim composition that is depleted in HREE+Y (Fig. 6a and b). Both types of garnet have roughly similar grain sizes and equally spaced ionprobe spots. Therefore, both analysed garnets are comparable and, in contrast to the inclusion-rich garnet, the HREE+Y-enriched core composition of the inclusion-poor garnet appears to be somewhat larger than the HREE+Y-depleted rim. Core–rim variation of HREE+Y is also gradual, but in contrast to the inclusion-rich garnet, the inclusion-poor garnet has a core composition that is slightly depleted in HREE+Y and also displays HREE enrichment at the outermost rim. Ignoring the HREE-enriched outermost rim, HREE concentrations are similar to both garnet types. In

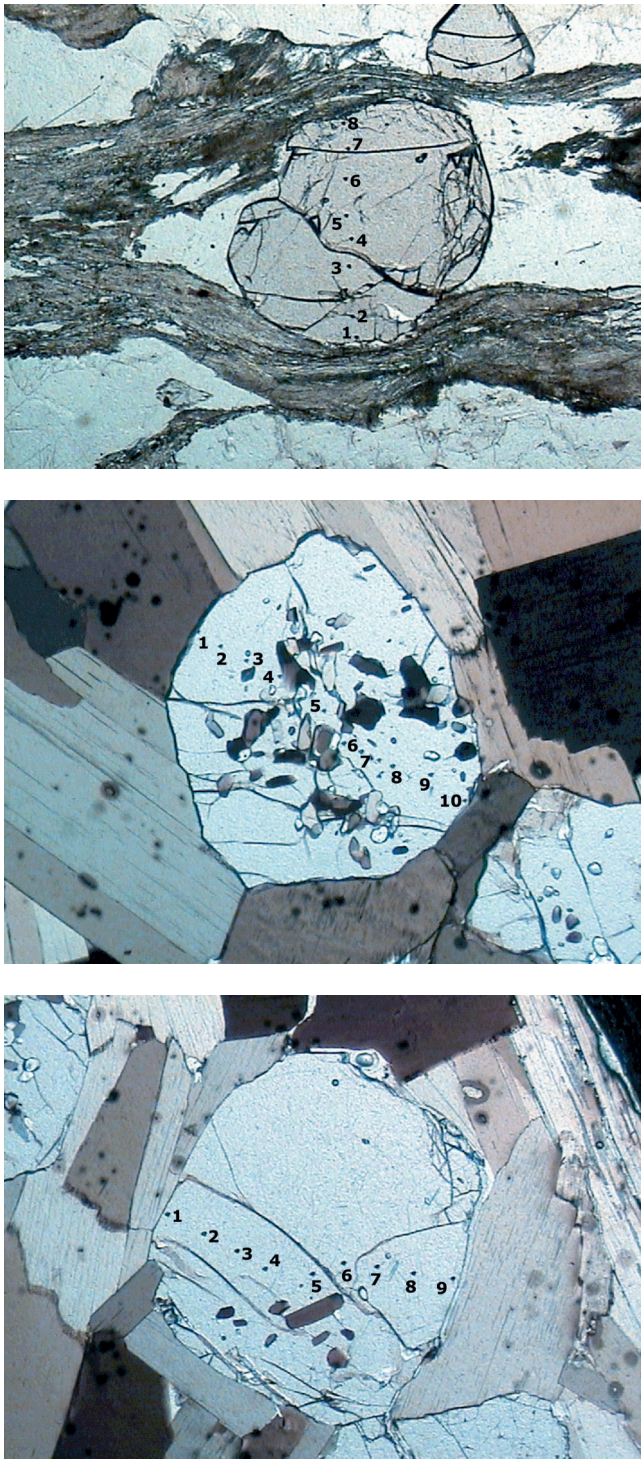

Figure 3 Photographs of garnet from the different samples with the approximate location of the spots analysed by ion microprobe: (top) inclusion-rich garnet from melanosome MEL 3; (middle) inclusion-poor garnet from melanosome MEL 3; (bottom) inclusion-free garnet from leucosome LEU 3. Lower side of each photograph is approximately 2 mm.

https://doi.org/10.1017/S1755691009016107 Published online by Cambridge University Press

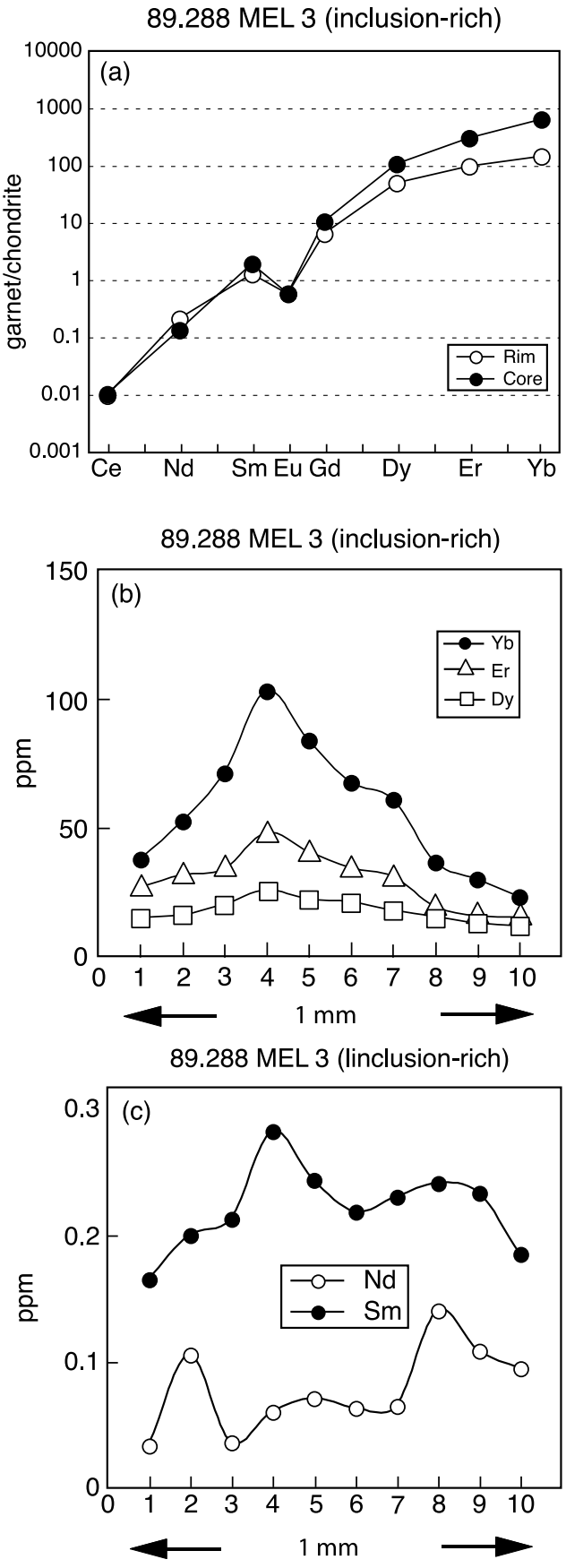

Figure 4 (a) Chondrite-normalised Rare Earth Element plot for core and rim for inclusion-rich garnet from melanosome MEL 3. (b) HREE variation along a rim-core–rim profile. (c) Sm and Nd variation along a rim-core–rim profile. Chondrite values are from Boynton (1984).

contrast to the inclusion-rich garnet from the melanosome, REE zoning is similar for the MREE (rim/core ~0·3–0·8 for Sm, Eu, Gd), and for the more compatible HREE (rim/core ~0·3–0·7 for Dy–Yb) and Y (rim/core: 0·3). Whereas in the inclusion-rich garnet, the core–rim distribution increases from Yb (core/rim: 0·22) and Er (core/rim: 0·32) to Dy (core/rim: 0·46), the core–rim variation in the inclusion-poor garnet decreases from Yb (core/rim: 0·68), Er (core/rim: 0·45) and Dy (core/rim: 0·28). Yttrium concentrations are similar at the outermost rim of both garnet types, but are enriched by a factor of two in the core of the inclusion-poor garnet. In contrast to the inclusion-rich garnet from the melanosome, concentration profiles for Ti, V, Cr, Zr and Sr show enriched core compositions and depleted rim compositions. Zr abundances are highly symmetric and cannot be explained by contamination with micro-inclusions of zircon. For Ti, there is a pronounced peak in the core region, whereas the concentration profiles for V, Cr, and Zr are rather flat. Sr displays re-enrichment at the outermost rim. Sc shows a rather flat concentration profile, with lower concentrations in the core than in the rim (Table 1). The distribution of Sm and Nd follows roughly that for HREE and Y, with low values in the core region followed by enrichment of Sm and Nd at the rim. At the outermost rim, Sm and Nd concentrations are significantly lower (Fig. 6c). Fractionation of LREE ($(Sm/Nd)_N$) shows a core with lower ratios and a rim with higher ratios. The outermost rim shows significantly lower ratios than both, core and rim. Fractionation of HREE (Yb/Dy and Yb/Er ratios) shows elevated ratios in the core and lower values in the rim. The outermost rim shows significantly higher ratios than in the core and rim (Fig. 7). The magnitude of the negative Eu anomaly ranges from 0·01 to 0·06 with a tendency to decrease towards the rim.

4.2.3. Inclusion-free garnet (leucosome). Like the other two garnet types from the melanosome, the garnet from the leucosome has a core composition enriched in HREE+Y and a rim composition that is depleted in HREE+Y (Fig. 8a, b). Compared to the other garnet, the trace element-enriched core region is only 1/3 that of the total garnet. Rare Earth Element zoning is similar or less pronounced for the middle REE (rim/core ~0·3–0·7 for Sm, Eu, Gd), compared to the more compatible heavy REE (rim/core ~0·3–0·2 for Dy–Yb) and Y (rim/core: 0·3). The core–rim variation in HREE and Y is gradual. In contrast to the other garnets, other trace elements exhibit either pronounced core–rim depletion (Sr, Zr, Sc) or core–rim enrichment (Ti, V, Cr, Na; Table 1). Again, the core is enriched in Zr. If contamination by micro-inclusions is responsible for this selective enrichment, it would be highly fortuitous that this occurred exactly in the core region. In some cases, elements may show enrichment (Sc) or depletion (Na) at the outermost rim. The distribution of Sm and Nd follows roughly that for HREE and Y, with high values in the core region followed by depletion of Sm and Nd at the rim. At the outermost rim, Sm and Nd concentrations are slightly enriched (Fig. 8c). Fractionation of LREE ($(Sm/Nd)_N$) shows a core with lower ratios and a rim with higher ratios. Fractionation of HREE (Yb/Dy and Yb/Er ratios) shows low ratios in the core followed by elevated values towards the rim. The outermost rim shows similar low ratios than in the core (Fig. 9). As in the inclusion-poor garnet from the melanosome, the magnitude of the negative Eu anomaly ranges from 0·01 to 0·06, with a tendency to decrease towards the rim.

5. Discussion

5.1. Garnet Gd/Dy geothermometry

Heavy Rare Earth Element variation, i.e. the Gd/Dy ratio, can be used to constrain the equilibration pressure that prevailed

https://doi.org/10.1017/S1755691009016107 Published online by Cambridge University Press

Table 1 Trace element composition (in ppm) of garnet from melanosome MEL 3 and leucosome LEU 3. For sample reference see Jung *et al.* (1998).

Inclusion-rich garnet MEL 3	Rim			Core						Rim
Na	90·2	87·9	54·8	49·0	47·5	87·5	144	141	105	120
Sc	140	155	141	164	157	147	137	135	144	124
Ti	17·5	22·8	23·0	23·7	23·2	29·0	34·1	55·1	50·8	40·6
V	18·6	19·8	14·3	13·7	13·6	15·1	17·8	20·7	18·2	17·8
Cr	67·7	79·3	74·1	70·5	66·6	76·9	88·5	79·6	70·5	87·2
Sr	0·16	0·15	0·17	0·17	0·17	0·16	0·15	0·15	0·15	0·15
Y	161	187	209	287	241	227	199	168	133	139
Zr	12·2	14·2	3·8	3·80	2·12	24·3	41·0	82·9	55·1	50·2
La	0·01	0·11	0·00	0·00	0·00	0·00	0·00	0·00	0·00	0·00
Ce	0·01	0·18	0·01	0·01	0·00	0·00	0·00	0·01	0·00	0·01
Nd	0·03	0·11	0·04	0·06	0·07	0·06	0·07	0·14	0·11	0·09
Sm	0·17	0·20	0·21	0·28	0·24	0·22	0·23	0·24	0·23	0·19
Eu	0·027	0·014	0·024	0·032	0·025	0·029	0·016	0·026	0·045	0·032
Gd	1·28	1·32	1·60	2·06	1·94	1·78	1·34	1·54	1·45	1·26
Dy	15·0	16·2	20·2	25·7	22·3	21·1	17·9	15·4	12·9	11·9
Er	26·8	31·7	33·8	47·9	40·7	34·3	31·0	19·3	15·7	15·3
Yb	37·7	52·4	71·1	103·0	83·9	67·6	60·9	36·6	30·0	23·2
Sm/Nd(N)	4·9	1·9	5·9	4·7	3·4	3·5	3·5	1·7	2·1	2·0
Yb/Dy	2·5	3·2	3·5	4·0	3·8	3·2	3·4	2·4	2·3	1·9
Yb/Er	1·4	1·7	2·1	2·2	2·1	2·0	2·0	1·9	1·9	1·5

Inclusion-poor garnet MEL 3	Rim			Core					Rim
Na	89·9	95·6	83·6	90·2	96·4	94·9	87·4	80·9	71·9
Sc	124	88·0	91·5	98·6	97·8	104	107	122	149
Ti	41·9	161	202	164	613	123	101	217	40·8
V	15·9	19·2	21·3	24·3	23·4	23·2	25·2	23·3	16·7
Cr	81·5	104	105	124	113	114	101	91·2	83·6
Sr	0·19	0·16	0·18	0·20	0·23	0·24	0·18	0·18	0·23
Y	179	182	422	606	544	654	534	401	406
Zr	16·9	45·0	55·2	55·8	53·2	54·5	53·4	56·1	13·1
La	0·00	0·00	0·01	0·01	0·01	0·00	0·01	0·00	0·01
Ce	0·00	0·01	0·01	0·01	0·01	0·01	0·02	0·01	0·01
Nd	0·06	0·18	0·29	0·23	0·12	0·15	0·21	0·34	0·09
Sm	0·27	0·71	1·57	1·20	0·66	0·84	1·00	1·69	0·26
Eu	0·035	0·084	0·101	0·034	0·044	0·040	0·035	0·095	0·025
Gd	2·41	4·93	10·9	11·1	8·41	9·78	11·2	11·8	3·43
Dy	20·2	28·0	64·9	83·2	71·6	86·0	81·5	60·7	44·9
Er	33·7	21·6	44·4	83·0	73·7	90·3	55·8	39·4	102
Yb	69·7	22·7	43·0	107	102	124	50·5	36·7	220
Sm/Nd(N)	4·8	4·0	5·3	5·3	5·6	5·4	4·7	5·0	2·8
Yb/Dy	3·4	0·8	0·7	1·3	1·4	1·4	0·6	0·6	4·9
Yb/Er	2·1	1·0	1·0	1·3	1·4	1·4	0·9	0·9	2·2

during formation of the garnet (Bea *et al.* 1997). The studied garnets from the melanosome and leucosome show Gd and Dy zoning similar to the zoning observed for the more compatible HREE and, consequently, this type of zoning is interpreted to be the result of Rayleigh-type fractionation during growth of the garnet. It seems that Gd and Dy behave similarly and therefore Gd/Dy ratios are fairly constant over the crystal. Using the equation derived by Bea *et al.* (1997), average apparent equilibration pressures are $4{\cdot}1 \pm 0{\cdot}04$ kbar for the inclusion-rich garnet from the melanosome, $4{\cdot}4 \pm 0{\cdot}2$ kbar for the inclusion-poor garnet from the melanosome and $4{\cdot}2 \pm 0{\cdot}1$ kbar for the inclusion-free garnet from the leucosome. These pressures are slightly lower than the pressures of $5{\cdot}2 \pm 0{\cdot}4$ kbar and $5{\cdot}6 \pm 0{\cdot}2$ kbar obtained by conventional GASP and Grt–Crd cation exchange barometry (Jung *et al.* 1998).

5.2. Inclusion-rich garnet (melanosome)

The inclusion-rich garnet from the melanosome is part of a restitic mineral assemblage consisting of garnet, biotite, sillimanite, spinel and quartz (Jung *et al.* 1998). Based on distinct Sm–Nd garnet-whole rock ages and U–Pb monazite ages, the migmatite is considered to have undergone multiple high-grade episodes, including one or more metamorphic and/or anatectic events. With respect to the garnet, it is likely that the actual mineralogical composition of the melanosome records only the latter of these episodes. This suggestion is supported by a Sm–Nd garnet whole rock age of 488 ± 9 Ma, which is the youngest age among the different parts of the migmatite (Jung & Mezger 2001). Therefore, it is suggested that the garnet trace element composition can be used to place constraints on the garnet-forming process, namely growth of garnet in a closed system with no change in garnet growth reaction. In theory,

https://doi.org/10.1017/S1755691009016107 Published online by Cambridge University Press

Table 1 *Continued.*

Inclusion-free garnet LEU 3	Rim			Core				Rim
Na	99·3	113	140	80·8	84·7	71·9	111	95·8
Sc	113	87·6	82·7	144	109	116	111	139
Ti	54·2	43·7	34·1	31·0	35·3	40·5	62·1	52·9
V	33·8	16·9	20·3	9·6	23·1	19·3	24·2	26·4
Cr	14·9	15·2	14·7	7·83	15·2	14·0	13·3	9·80
Sr	0·12	0·10	0·12	0·17	0·16	0·13	0·11	0·11
Y	163	103	130	553	274	149	99·5	167
Zr	7·41	7·50	8·60	63·5	8·58	3·65	10·5	13·7
La	0·00	0·00	0·00	0·00	0·00	0·00	0·00	0·00
Ce	0·01	0·00	0·00	0·00	0·01	0·01	0·01	0·00
Nd	0·07	0·03	0·04	0·13	0·05	0·09	0·07	0·06
Sm	0·21	0·14	0·14	0·52	0·30	0·16	0·16	0·28
Eu	0·02	0·02	0·01	0·02	0·02	0·03	0·03	0·03
Gd	1·71	1·23	1·28	6·37	2·33	1·49	1·47	2·50
Dy	18·5	11·9	13·0	63·8	20·4	10·3	11·2	22·3
Er	16·8	14·1	17·3	76·8	31·3	14·7	13·0	21·3
Yb	27·2	27·6	40·0	135·4	73·2	25·7	15·3	34·2
Sm/Nd(N)	3·0	4·5	3·6	4·0	6·3	1·8	2·4	4·7
Yb/Dy	1·5	2·3	3·1	2·1	3·6	2·5	1·4	1·5
Yb/Er	1·6	2·0	2·3	1·8	2·3	1·7	1·2	1·6

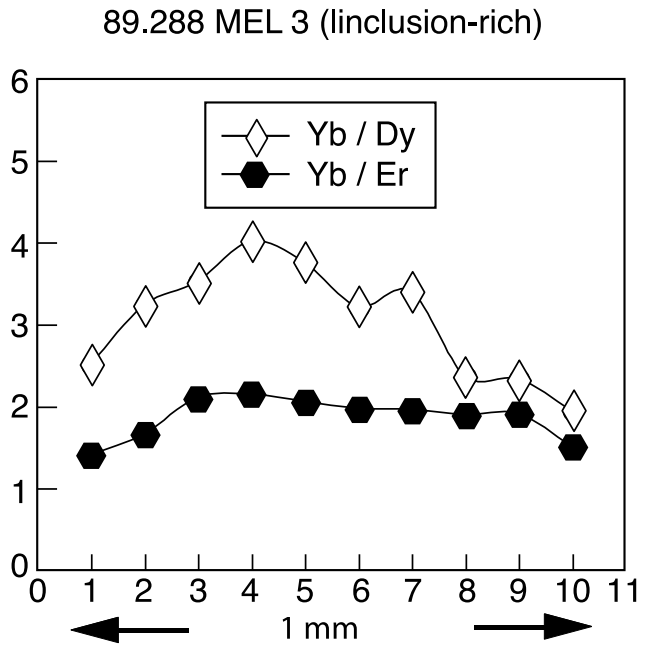

Figure 5 Yb/Dy and Yb/Er variation along the same profile for the inclusion-rich garnet from melanosome MEL 3.

the abundance of a trace element on the surface of a growing garnet in equilibrium with a surrounding metamorphic mineral assemblage is controlled by (i) the effective bulk composition and (ii) the bulk distribution coefficient (Kd) for partitioning of the element between the garnet and the matrix phases. Therefore, the zoning of elements that exhibit decreasing (Sr, Y, HREE, Sm) concentrations from core to rim can be explained in terms of equilibrium closed-system partitioning models (Hollister 1966; Cygan & Lasaga 1982; Otamendi *et al.* 2002). In this model, crystal diffusion-controlled partitioning is a Rayleigh fractionation process, whereby surface equilibrium is maintained and elemental diffusion is limited by the growing crystal. This process assumes mass balance in the reservoir (i.e., a closed system which in this case is the metamorphic host rock), constant Kd values and removal of a fractionating element by mineral growth.

One interesting feature is the distribution of Nd relative to Sm. Nd is more incompatible than Sm in garnet, and in the core region, at the point where Sm peaks, Nd concentrations are low followed by re-enrichment towards the rim (Fig. 4c). This feature may indicate limited volume diffusion of Nd during high-temperature metamorphism.

Heavy Rare Earth Element fractionation, monitored by Yb/Dy and Yb/Er ratios, is continuous from core to rim and more pronounced for Yb/Dy than for Yb/Er ratios which is consistent with the different partition coefficient, $D^{garnet/matrix}$ such that $D_{Yb}>D_{Er}>D_{Dy}>D_{Gd}$ (Fig. 5). Otamendi *et al.* (2002) described garnet from an anatectic terrane in which residual garnet cores, interpreted to have grown during high-grade regional metamorphism, have high Yb/Er and Yb/Dy ratios. Garnet rims, interpreted as peritectic garnet, show inverted ratios, i.e., lower Yb/Dy and higher Yb/Er ratios. The most prominent feature of the HREE systematics was an inflection of the HREE ratios at the core–rim interface. The continuous decrease of HREE ratios in the inclusion-rich garnet from the melanosome may arise from equilibrium partitioning during garnet growth, but the missing inflection indicates that partial melting processes are not monitored by the garnet composition.

5.3. Inclusion-poor garnet (melanosome)

In contrast to the other garnet from the melanosome, this garnet has much fewer inclusions (Fig. 3b). Elements such as Sr, Ti, V and Cr show core–rim depletion, whereas Sc shows core–rim enrichment (Table 1). The distribution of these elements may indicate equilibrium closed-system partitioning (Rayleigh fractionation). Generally, Heavy Rare Earth Element and Y abundances decrease from core to rim (Fig. 6a). However, in the core region, there is a slight depletion in HREE and Y relative to the adjacent rim. In addition, the outermost rim shows re-enrichment in HREE and Y (Fig. 6b). The slight depletion in the core, followed by higher values at the rim with subsequent depletion and re-enrichment at the outermost rim, suggests a multi-stage growth history. Taken

https://doi.org/10.1017/S1755691009016107 Published online by Cambridge University Press

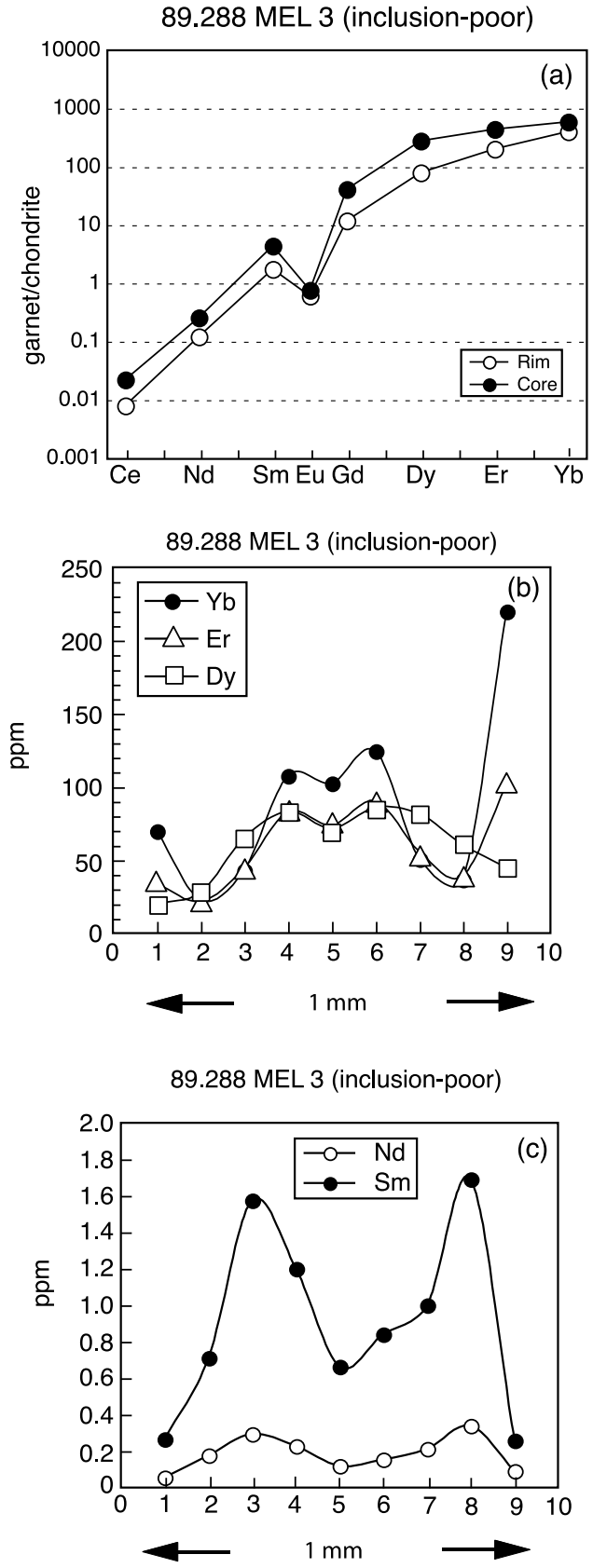

Figure 6 (a) Chondrite-normalised Rare Earth Element plot for core and rim for inclusion-poor garnet from melanosome MEL 3. (b) HREE variation along a rim-core–rim profile. (c) Sm and Nd variation along a rim-core–rim profile.

together, these features cannot reflect distribution of these elements following an equilibrium closed-system partitioning model.

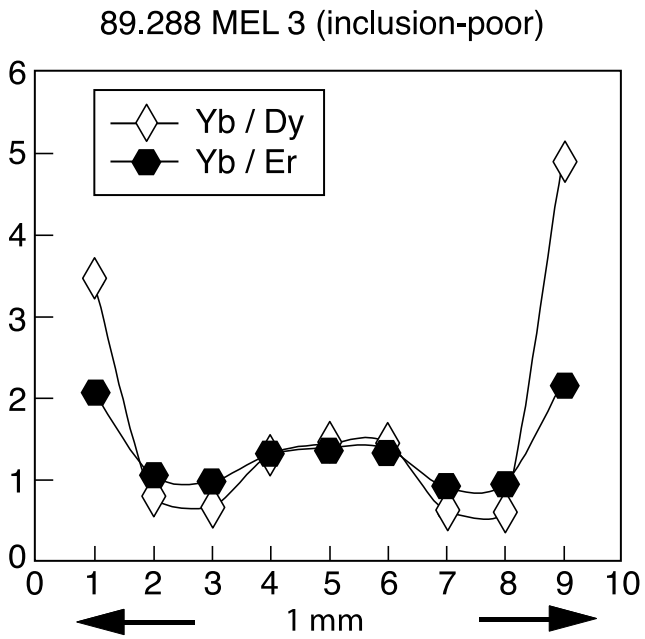

Figure 7 Yb/Dy and Yb/Er variation along the same profile for the inclusion-poor garnet from melanosome MEL 3.

It is possible that the core–rim distribution of HREE and Y can be attributed to variable garnet growth rates during high-grade metamorphism and melting. Variable garnet growth rates are possible because it is reasonable to assume that the garnet now preserved in the melanosome has, in part, started to grow within the melanosome matrix; but subsequently equilibrated with an *in-situ*-derived granitic melt where additional growth of this garnet took place. Such a process may explain the increase in HREE abundances towards the rim, because there is no sink for HREE in the inferred REE-depleted leucosome. If such a reaction indeed proceeded during migmatisation, changes in the phase assemblages are unavoidable because of the distinct mineralogical composition of the host melanosome and the *in situ*-derived melt. Such complex distributions patterns of enrichment/depletion of HREE and Y may indicate an episode of open system behaviour. In contrast to the inclusion-rich garnet from the melanosome, the inclusion-poor garnet shows a complex HREE fractionation pattern. In the core, Yb/Dy and Yb/Er ratios are high, with Yb/Dy>Yb/Er, which is consistent with partition coefficient $D_{garnet/matrix}$:D_{Yb}>D_{Er}>D_{Dy}. Subsequently, these ratios decrease towards the rim (Fig. 7). Towards the outermost rim, an inversion of these HREE ratios occur, with Yb/Dy<Yb/Er. Only the outermost rim shows Yb/Dy>Yb/Er. The inflection of these ratios between core and rim can be interpreted as a result of partial melting. Garnet cores with high Yb/Er and Yb/Dy>1 nucleated in the metamorphic environment without the presence of a melt, whereas the rims with lower Yb/Er and Yb/Dy<1 crystallised in the presence of a melt (Otamendi *et al.* 2002).

5.4. Inclusion-free garnet (leucosome)

Based on the apparent lack of inclusions, it can be suggested that this garnet is distinct to the other two garnets and probably equilibrated in the presence of a melt. The zoning of elements that exhibit either decreasing concentrations (LREE, HREE, Y, Sr, Zr, Sc) or increasing concentrations (Ti, V, Cr, Na) from core to rim can be explained in terms of a near-equilibrium closed-system partitioning model. Similar to the model that is suggested for the inclusion-rich garnet from the melanosome, crystal diffusion-controlled partitioning is a

https://doi.org/10.1017/S1755691009016107 Published online by Cambridge University Press

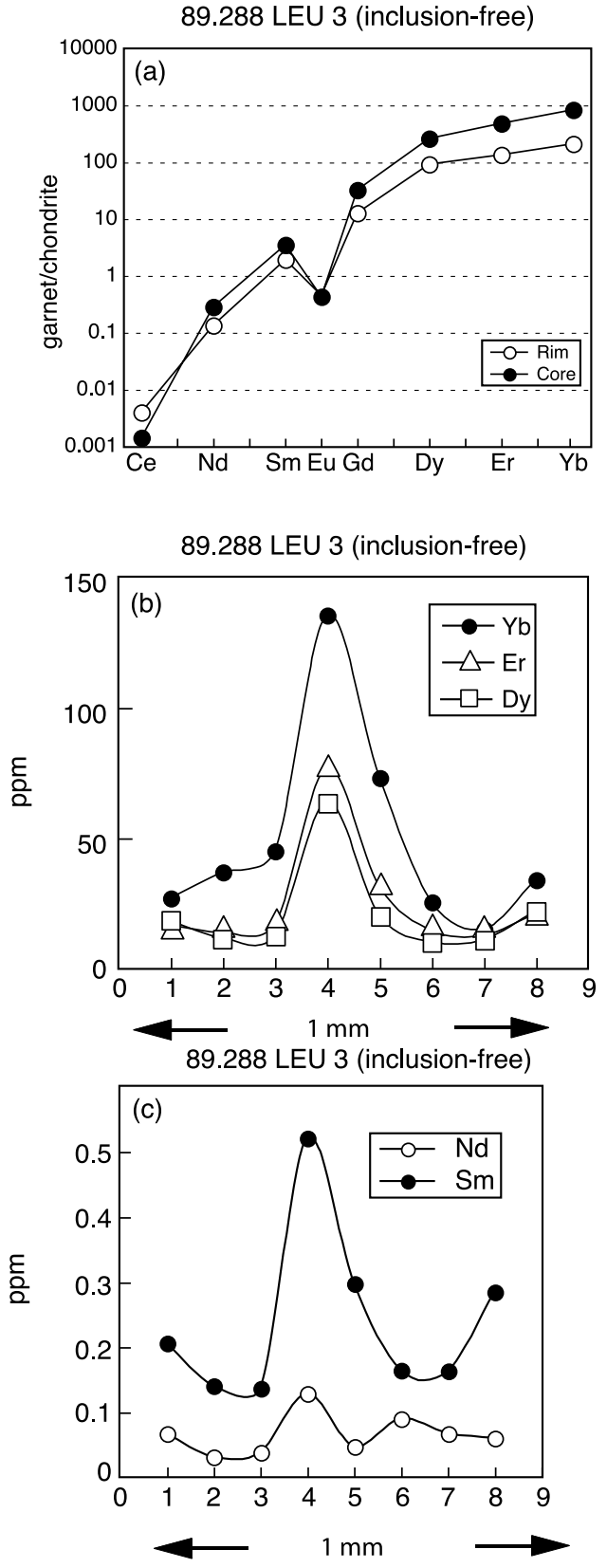

Figure 8 (a) Chondrite-normalised Rare Earth Element plot for core and rim for inclusion-free garnet from leucosome LEU 3. (b) HREE variation along a rim-core–rim profile. (c) Sm and Nd variation along a rim-core–rim profile.

Rayleigh fractionation process, whereby surface equilibrium is maintained and elemental diffusion is limited by the growing crystal. This process assumes mass balance in the reservoir (i.e., a closed system which in this case is the leucosome), constant Kd values and removal of a fractionating element by

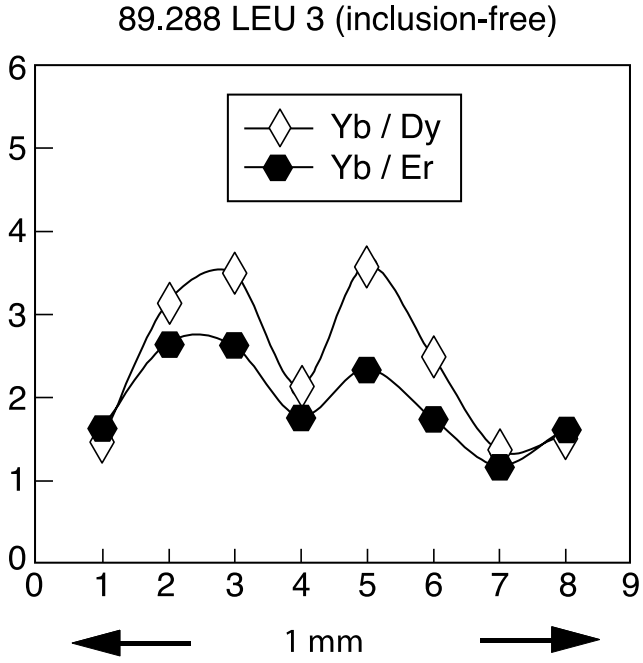

Figure 9 Yb/Dy and Yb/Er variation along the same profile for the inclusion-free garnet from leucosome LEU 3.

mineral growth. In the initial stages of garnet growth, the relatively small core of the garnet nucleated and acted as a sink for the most compatible trace elements (i.e., HREE, Y) that show decreasing concentrations from core to rim (Figs 8 & 9). Subsequently, the volumetrically much larger and trace element-depleted rim crystallised in equilibration with the LREE-depleted leucosome. The lower Yb/Dy and Yb/Er in the core are enigmatic; one possible explanation could be that the core region represents an entrained, restitic garnet from the melanosome. However, textural evidence does not support such a suggestion.

The accurate interpretation of trace element variation in garnet coexisting with a granitic liquid has important implications for trace element behaviour during partial melting processes. In general, garnet that crystallised in the presence of a melt is distinct to garnet from metamorphic environments. In contrast to garnet from strongly fractionated leucogranite (Sevigny 1993; Jung & Hellebrand 2006), the garnet from the leucosome shows a trace element distribution similar to those observed in garnet from high-grade metamorphic or migmatitic rocks. Due to the observation that the leucosome garnet is inclusion-free, incorporation of this garnet from the melanosome into the leucosome seems to be precluded. This implies that the process that formed the trace element pattern of the leucosome garnet was distinct from the liquid diffusion controlled process (i.e., Sevigny 1993) envisaged for leucogranitic garnets. One possible explanation could be that in hot, highly viscous, H_2O-poor leucosomes from high-grade terranes, the rate of diffusion of trace elements is similar to the rate envisaged for high-grade metamorphic rocks, but distinct to the rate suggested for fluid-dominated leucogranites.

5.5. Implications for the HREE composition of garnet-bearing leucosomes

It has been suggested that the HREE composition of metamorphic and peritectic garnet can be used to make assumptions about equilibration of garnet with *in situ*-derived melts (Otamendi *et al.* 2002). Here, the inflection of the Yb/Dy and Yb/Er ratios at the interface between garnet core and rim was interpreted as to result from partial melting processes in which

https://doi.org/10.1017/S1755691009016107 Published online by Cambridge University Press

the garnet core with its characteristic high Yb/Dy ratios nucleated in the metamorphic environment and the rim with lower Yb/Dy ratios nucleated in an environment that is characterised by HREE depletion, i.e. representing an *in situ* partial melt. Therefore, calculated REE patterns of the inferred *in situ* melts can show a marked hump at Yb, using garnet core compositions and melts equilibrated with the rim that are depleted in Yb relative to Y and Er (see figure 3 of Otamendi *et al*. 2002 for reference). Since the inclusion-poor garnet from the melanosome and the inclusion-free garnet from the leucosome show some of these features (inverted Yb/Dy and Yb/Er ratios at the core–rim interface), it is pertinent to calculate corresponding leucosome compositions and to compare them with the leucosomes from the migmatite and with granitic melts from the Damara orogen.

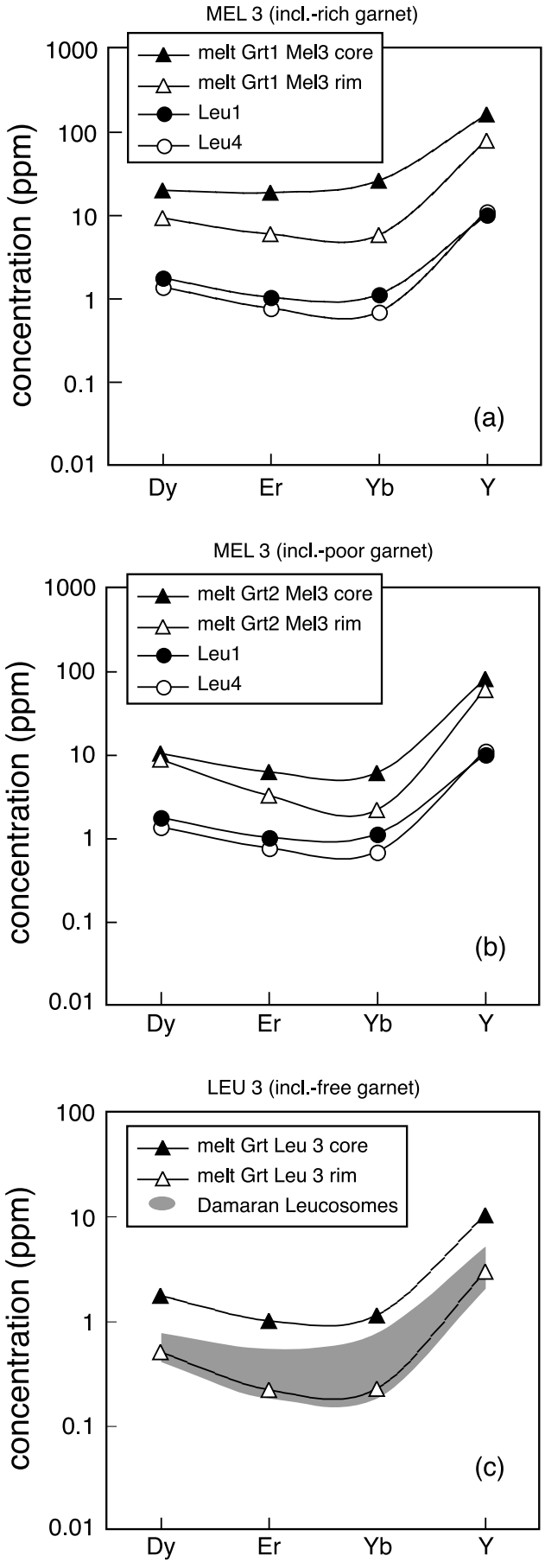

Figure 10a–c shows multi-element distribution pattern for equilibrium partial melts calculated from the garnet composition (core and rim) using calculated mineral-melt distribution coefficients according to the approach of Hollister (1966). From Figure 10a it is obvious that, for the inclusion-rich garnet from the melanosome, calculated compositions of corresponding felsic melts either in equilibrium with the garnet core or the rim are one order of magnitude higher in HREE and Y relative to unfractionated leucosomes from the migmatite. These features may indicate that this garnet was never in equilibrium with a felsic melt similar in composition to unfractionated leucosomes from the migmatite. In the case of the inclusion-poor garnet from the melanosome, the calculated melt compositions are also enriched in HREE and Y, but the rim composition tend to approach the composition of the leucosomes from the outcrop.

For the inclusion-free garnet from the leucosome, the melt composition calculated with the core composition of the garnet is markedly enriched in HREE and Y. On the other hand, the melt composition that is calculated using the garnet rim composition is depleted in HREE and Y, and is similar to other leucosome compositions from the Damara orogen. Based on the data of Otamendi *et al*. (2002), it was concluded that *in situ*-derived felsic melts were unable to equilibrate with garnet cores, but were able to equilibrate with garnet rims. Some of the features interpreted to be characteristic for peritectic garnet (i.e., inversion of Yb/Dy and Yb/Er ratios at the core–rim interface) are also observed in the migmatite garnets from the Davetsaub/Nomatsaus areas, and it seem also obvious that calculated melt compositions were in equilibrium with garnet rims but not the cores.

6. Conclusion

This study demonstrates that trace element zoning in garnet porphyroblasts from a polyphase migmatite from the high-grade part of the Damara orogen (Namibia) provide a powerful tool of investigating melting processes in the crust. Trace element zoning in garnet is more pronounced than major

Figure 10 Plots of calculated abundances of Dy, Er, Yb and Y in melts, assuming equilibration with either garnet cores or garnet rims. Assumptions for the calculation of the trace element abundances were (i) garnet is the only phase that govern these trace element abundances and (ii) bulk partition coefficients between garnet and matrix (melanosome or leucosome) are similar to partition coefficients between garnet and melt. The latter assumption is an oversimplification, but actual garnet/melt partition coefficients are likely to be similar to garnet/matrix partition coefficients and relative values of partition coefficients such as ($D_{Yb}>D_{Er}>D_{Y}>D_{Dy}$). Because of the large values for D, melt fraction has a minor effect on calculated trace element concentrations in the melt and, therefore, garnet/melt partitioning can be simplified to: $C(i)_{melt}/C(i)_{garnet}=1/D(i)$, where $C(i)_{melt}$ and $C(i)_{garnet}$ are concentrations of an element (i) in melt and garnet, respectively. Also shown in (c) are trace element abundances in leucosomes from the Damara orogen (Jung *et al*. 2000, 2003).

https://doi.org/10.1017/S1755691009016107 Published online by Cambridge University Press

element zoning, and provides information on important metamorphic processes, i.e. *in situ* migmatisation and metamorphic growth; information that cannot be retrieved from major-element investigations alone. As anticipated, the garnet analysed in this study are important reservoirs for HREE and Y. The concentrations of HREE and Y in garnet cores are in most cases the result of simple Rayleigh fractionation between the growing garnet and the rock matrix. The signatures of this process are the bell-shaped element distribution patterns. However, inclusion-poor garnet from a melanosome shows a more complex trace element pattern with distinct distribution patterns, suggesting disequilibrium between garnet and an inferred *in situ*-derived melt. Such complex trace element distribution patterns probably mark the onset of open system processes. The preservation of such disequilibrium patterns may occur when mineral growth rates are rapid, particularly in migmatite environments where temperature overstepping may occur. Reacting metamorphic minerals and *in situ*-derived melts have distinct trace element compositions, and because trace element diffusivities in garnet are apparently slow at amphibolite facies to lower granulite facies conditions, variations in garnet trace element compositions can be used to track the metamorphic history of such rocks.

7. Acknowledgements

This study was supported by a grant from the Deutsche Forschungsgemeinschaft to E. Hoffer (Ho 1078/12-1) and the Max-Planck Gesellschaft. The authors would like to thank G. Lugmair and Al Hofmann (MPI Mainz) for access to the ionprobe hosted by the Max Planck Institut für Chemie in Mainz. Peter Hoppe and Elmar Gröner are warmly thanked for keeping the ionprobe in good shape. I. Bambach is warmly thanked for producing high quality figures. We would like to thank I. Buick and F. Bea for the instructive reviews and editor G. Stevens for smooth and patient editorial handling.

8. Appendix. Analytical techniques

Garnet was analysed for trace elements (selected REE and Na, Sc, Ti, V, Cr, Sr, Y, Zr) by secondary ion mass spectrometry (SIMS) on a recently upgraded Cameca IMS-3f in Mainz. Spots were selected for ion microprobe analysis after detailed petrographic and electron microprobe study. Only optically clear domains that showed no signs of alteration or opx exsolution were analysed. Negative oxygen ions were used as primary ions (accelerating potential of 12·5 kV and 20 nA beam current). The spot size for these operating conditions was 15–20 μm. For very small grains, the beam current was reduced to 10 nA, resulting in a smaller spot size (around 10 μm). Positive secondary ions were extracted using an accelerating potential of 4·5 kV with a 25 eV energy window, a high-energy offset of -80 V, and fully open entrance and exit slits. Each measurement consisted of a six-cycle routine, where in each cycle the species ^{16}O, ^{30}Si, ^{47}Ti, ^{51}V, ^{52}Cr, ^{88}Sr, ^{89}Y, ^{90}Zr, ^{138}Ba, ^{139}La, ^{140}Ce, ^{146}Nd, ^{147}Sm, ^{153}Eu, ^{157}Gd, ^{163}Dy, ^{167}Er and ^{174}Yb were analysed, in that order. In each cycle, the REE were measured for 30 s, Sr, Zr and Ba for 20 s, Ti, V and Y for 5 s, and the other elements for 1 s. At the beginning of each analysis, the energy distribution of ^{16}O was measured to determine the maximum intensity and the precise location of the 10% low-energy edge of the distribution. The location of this sharp edge can be determined more precisely than the location of relatively broad maximum intensity. Given that $U_{\text{max-edge}}$ is +20 V, the applied high-energy offset is about -100 V from the location of the 10% value of this steep flank. In this way, differences in ion energy as a result of charge build-up from one sample to the next do not affect the energy range of the ions being analysed (Zinner & Crozaz 1986). Subsequently, peak centres were determined for ^{30}Si, ^{47}Ti, ^{89}Y and ^{163}Dy by scanning the peak in 20 steps across a 1·5 wide B-field. The neighbouring masses (Cr and V on Ti, Sr and Zr on Y, and all REE on Dy) were then adjusted to these new peak centres. From one measurement to the next, however, the peak shift was rarely significant (<50 ppm). For all silicates, ^{30}Si (3·1% isotopic abundance) is used as a reference mass, as the SiO_2 concentration of standards and samples is known from electron microprobe analysis. For each cycle, mass to ^{30}Si ratios were determined after correction for time-dependence of count rates, detector deadtime (20 ms) and background [10^{-3} c.p.s. (counts per second)]. The average of these ratios was used to calculate the element concentration, multiplying the measured ratios by a constant factor. These so-called sensitivity factors were determined for each element on the well-studied standard glasses KL2–G, ML3B-G, StHs6/80–G, BM90/21–G and ATHO-G (Jochum *et al.* 2000). For this purpose, a different measurement routine that determines the mass spectrum between 133 and 191 was adopted (Zinner & Crozaz 1986), referred to below as the 'long routine'. This approach is necessary to obtain accurate sensitivity factors for the REE. Although the applied energy filtering technique (Shimizu *et al.* 1978) eliminates the effect of most molecular interferences, it is well known that element monoxides can produce significant interferences, particularly on REE (e.g. PrO on Gd). These have to be corrected. The intensity of an interfering oxide is a function of three parameters: the absolute concentration element of the interfering oxide (i.e. shape of the REE pattern), its isotopic abundance, and the oxide/element ratio of the interfering species. In contrast to the short routine described above, the long routine provides an internally consistent method to determine the corrected element/Si ratios and the oxide/element ratio. A detailed description of this iterative data reduction procedure was presented by Zinner & Crozaz (1986). Owing to the low LREE concentrations in garnet, the short measurement routine was preferred over the long routine, as the poor counting statistics at the extremely low counting rates caused an unacceptable propagating error and long duration time for a single analysis. Therefore, the short routine used the MO^+/M^+ values obtained by the long routine. Furthermore, six oxides were found to produce significant interferences: $^{137}BaO^+$ interferes with $^{153}Eu^+$, $^{141}PrO^+$ with $^{157}Gd^+$, $^{147}SmO^+$ with $^{163}Dy^+$, $^{151}EuO^+$ with $^{167}Er^+$, and both $^{158}GdO^+$ and $^{158}DyO^+$ with $^{174}Yb^+$, and their MO^+ to M^+ ratios used for the corrections are 0·046, 0·13, 0·06, 0·05, 0·08 and 0·07, respectively (with errors <10%). As all elements of these oxides are free of interferences, they were measured directly. For the concentrations of Eu, Gd, Dy and Er in a typical LREE-depleted garnet, these corrections were always <2% of the measured element/Si ratio. For Yb, the correction was 11%. The well-studied glass GOR132–G (Jochum *et al.* 2000) was used as an external standard, as its LREE-depleted pattern is broadly similar to that of the measured garnet (Table 1). The overall accuracy is between 7% and 19% for the REE and better than 11% for all other elements (95% confidence level). To distinguish 'real' counts from background noise at extremely low counting rates, separate background measurements with long counting times of between 10 and 30 min were carried out. All reported analyses are corrected for the background, which lies around 10^{-3} (c.p.s.) on average. The background concentration for each element that is based on such a count rate is controlled primarily by the intensity of ^{30}Si, which was (1·0–1·3) × 10^5 c.p.s. Defining a conservative

https://doi.org/10.1017/S1755691009016107 Published online by Cambridge University Press

detection limit at the six-fold background level, this corresponds to values for the REE that range from 0·6 ng/g (La) to 4 ng/g (Sm).

9. References

Bea, F., Montero, P., Garuti, G. & Zacharini, F. 1997. Pressure-dependence of rare-earth element distribution in amphibolite- and granulite-grade garnets. A LA-ICP-MS study. *Geostandards Newsletters* **21**, 253–70.

Blaxland, A., Gohn, E., Haack, U. & Hoffer, E. 1979. Rb/Sr ages of late-tectonic granites in the Damara orogen, Southwest Africa/Namibia. *Neues Jahrbuch für Mineralogie Monatshefte* **11**, 498–508.

Boynton, W. V. 1984. Geochemistry of rare earth elements: Meterorite studies. *In* Henderson, P. (ed.) *Rare earth element geochemistry*, 63–114. Amsterdam: Elsevier.

Brown, M. 1983. The petrogenesis of some migmatites from the Presqu'ile de Rhuys, Southern Brittany, France. *In* Atherton, M. P. & Gribble, C. D. (eds) *Migmatites, Melting and Metamorphism* 174–200. Nantwich: Shiva Press.

Chernoff, C. B. & Carlson, W. D. 1999. Trace element zoning as a record of chemical disequilibrium during garnet growth. *Geology* **27**, 555–8.

Cygan, R. & Lasaga, A. C. 1982. Crystal growth and the formation of chemical zoning in garnet. *Contributions to Mineralogy and Petrology* **79**, 187–200.

Essene, E. J. 1989. The current status of thermobarometry in metamorphic rocks. *In* Daly, J. S., Cliff, R. A. & Yardley, B. W. D. (eds) *Evolution of metamorphic belts. Geological Society, London, Special Publication* **43**, 1–44. Bath, UK: The Geological Society Publishing House.

Gray, D. R., Foster, D. A., Goscombe, B., Passchier, C. W. & Trouw, R. A. J. 2006. Ar^{40}/Ar^{39} thermochronology of the Pan-African Damara Orogen, Namibia, with implications for tectonothermal and geodynamic evolution. *Precambrian Research* **150**, 49–72.

Haack, U., Hoefs, J. & Gohn, E. 1982. Constraints on the origin of Damaran granites by Rb/Sr and $\delta^{18}O$ data. *Contributions to Mineralogy and Petrology* **79**, 279–89.

Hartmann, O., Hoffer, E. & Haack, U. 1983. Regional metamorphism in the Damara orogen: Interaction of crustal motion and heat transfer. *In* Miller, R. McG. (ed.) *Evolution of the Damara orogen. Special Publication of the Geological Society, South Africa* **11**, 233–41.

Hickmott, D. D., Shimizu, N., Spear, F. S. & Selverstone, J. 1987. Trace element zoning in a metamorphic garnet. *Geology* **15**, 573–6.

Hickmott, D. D. & Shimizu, N. 1990. Trace element zoning in garnet from the Kwoiek area, British Columbia: disequilibrium partitioning during garnet growth? *Contributions to Mineralogy and Petrology* **104**, 619–30.

Hickmott, D. D. & Spear, F. S. 1992. Major and trace element zoning in metamorphic garnets from western Massachusetts. *Journal of Petrology* **33**, 965–1005.

Hoernes, S. & Hoffer, E. 1979. Equilibrium relations of prograde metamorphic mineral assemblages – a stable isotope study of rocks of the Damara orogen. *Contributions to Mineralogy and Petrology* **68**, 377–89.

Hollister, L. S. 1966. Garnet zoning: an interpretation based on the Rayleigh fractionation model. *Science* **154**, 1647–51.

Jochum, K. P., Dingwell, D. B., Rocholl, A., Stoll, B., Hofmann, A. W., Becker, S., Besmehn, A., Dietze, H.-J., Dulski, P., Erzinger, J., Hellebrand, E., Hoppe, P., Horn, I., Janssens, K., Jenner, G. A., Klein, M., McDonough, W. F., Maetz, M., Mezger, K., Münker, C., Nikogosian, I. K., Pickhardt, C., Raczek, I., Rhede, D., Seufert, H. M., Simakin, S. G., Sobolev, A. V., Spettel, B., Straub, S., Vincze, L., Wallianos, A., Weckwerth, G., Weyer, S., Wolf, D. & Zimmer, D. 2000. The preparation and preliminary characterisation of eight geological MPI-DING standard reference glasses for in-situ microanalysis. *Geostandards Newsletter* **24**, 87–133.

Jung, S. 2005. Garnet and staurolite as potential geochronometers in low to medium grade metamorphic rocks – U/Pb and Pb/Pb garnet and staurolite ages from the Southern Damara orogen (Namibia). *Geophysical Research Abstracts* **7**, EGU05–A-06266.

Jung, S., Mezger, K., Masberg, P, Hoffer, E. & Hoernes, S. 1998. Petrology of an intrusion-related high-grade migmatite: implications for partial melting of metasedimentary rocks and leucosome-forming processes. *Journal of Metamorphic Geology* **16**, 425–45.

Jung, S., Hoernes, S., Masberg, P. & Hoffer, E. 1999. The petrogenesis of some migmatites and granites (Central Damara orogen, Namibia): Evidence for disequilibrium melting, wall-rock contamination and crystal fractionation. *Journal of Petrology* **40**, 1241–69.

Jung, S., Hoernes, S. & Mezger, K. 2000. Geochronology and petrology of stromatic and nebulitic migmatites from the Proterozoic Damara Belt – importance of episodic fluid-present disequilibrium melting and consequences for granite petrology. *Lithos* **51**, 153–79.

Jung, S., Hoernes, S. & Mezger, K. 2003. Petrology of basement-dominated terranes: II. Contrasting isotopic (Sr, Nd, Pb, and O) signatures of basement-derived granites and constraints on the source region of granite (Damara orogen, Namibia) *Chemical Geology* **199**, 1–28.

Jung, S. & Hellebrand, E. 2006. Trace element fractionation during high-grade metamorphism and crustal melting – constraints from ion microprobe data of metapelitic, migmatitic and igneous garnets and implications for Sm–Nd garnet geochronology. *Lithos* **87**, 193–213.

Jung, S. & Mezger, K. 2001. Geochronology in migmatites – An Sm–Nd, U–Pb and Rb–Sr study from the Proterozoic Damara belt (Namibia) and implications for polyphase development of migmatites in high-grade terranes. *Journal of Metamorphic Geology* **19**, 77–9.

Jung, S. & Mezger, K. 2003. Petrology of basement-dominated terranes: I. Regionalmetamorphic P–T–t path from U–Pb monazite and Sm–Nd garnet geochronology (Central Damara orogen, Namibia). *Chemical Geology* **198**, 223–47.

Kukla, C. 1993. Strontium isotope heterogeneities in amphibolite facies, banded metasediments – a case study from the late Proterozoic Kuiseb Formation of the Southern Damara orogen, Central Namibia. *Memoirs of the Geological Survey Namibia* **15**, 1–139.

Kukla, C., Kramm, U., Kukla, P. A. & Okrusch, M. 1991. U–Pb monazite data relating to metamorphism and granite intrusion in the northwestern Khomas Trough, Damara Orogen, central Namibia. *Communications of the Geological Survey of Namibia* **7**, 49–54.

Masberg, H. P., Hoffer, E. & Hoernes, S. 1992. Microfabrics indicating granulite-facies metamorphism in the low-pressure central Damara Orogen, Namibia. *Precambrian Research* **55**, 243–57.

Miller, R. McG. 1983. The Pan-African Damara Orogen of South West Africa/Namibia: *In* Miller, R. McG. (ed.) *Evolution of the Damara orogen. Special Publication of the Geological Society, South Africa* **11**, 431–515.

Nieberding, F. 1976. Die Grenze der zentralen Granitzone südwestlich Otjimbingwe (Karibib Distrikt, Südwestafrika): Intrusionsverband, Tektonik, Petrographie. *Göttinger Arbeiten zur Geologie und Paläontologie* **19**, 1–78.

Otamendi, J. E., de la Rosa, J. D., Patino Douce, A. E. & Castro, A. 2002. Rayleigh fractionation of heavy rare earths and yttrium during metamorphic garnet growth. *Geology* **30**, 159–62.

Puhan, D. 1983. Temperature and pressure of metamorphism in the Central Damara orogen. *In* Miller, R. McG. (ed.) *Evolution of the Damara orogen. Special Publication of the Geological Society, South Africa* **11**, 219–23.

Saywer, E. W. 1981. Damaran structural and metamorphic geology in an area southeast of Walvisbay, SWA/Namibia. *Memoirs of the Geological Survey, South West Africa/Namibia* **7**, 1–94.

Sevigny, J. H. 1993. Monazite controlled Sm/Nd fractionation in leucogranites: An ion microprobe study of garnet phenocrysts. *Geochimica et Cosmochimica Acta* **57**, 4095–102.

Shimizu, N., Semet, M. P. & Allègre, J. C. 1978. Geochemical applications of quantitative ion microprobe analysis. *Geochimica et Cosmochimica Acta* **42**, 1321–34.

Spear, F. S., Hickmott, D., Crowley, P. & Hodges, K. V. 1984. P–T paths from garnet zoning: a new technique for deciphering tectonic processes in crystalline terrains. *Geology* **12**, 87–90.

Spear, F. S. & Florence, F. P. 1992. Thermobarometry in granulites: Pitfalls and new approaches. *Precambrian Research* **55**, 209–41.

Spear, F. S. & Kohn, M. J. 1996. Trace element zoning in garnet as a monitor of crustal melting. *Geology* **24**, 1099–102.

Spear, F. S. & Selverstone, J. 1983. Quantitative P–T paths from zones minerals: theory and tectonic implications. *Contributions to Mineralogy and Petrology* **83**, 348–57.

Thompson, A. B. 1982. Dehydration melting of pelitic rocks and the generation of H_2O-undersaturated granitic liquids. *American Journal of Science* **282**, 1567–95.

Tracy, R. J. 1982. Compositional zoning and inclusions in metamorphic minerals. *In* Ferry, J. M. (ed.) *Characterization of metamorphism through mineral assemblages in metamorphic rocks. Mineralogical Society of America Reviews in Mineralogy* **10**, 355–97.

Vielzeuf, D. 1983. The spinel and quartz associations in high grade xenoliths from Tallante (S.E. Spain) and their potential use in geothermometry and barometry. *Contributions to Mineralogy and Petrology* **82**, 301–11.

Ward, R., Stevens, G. & Kisters, A. 2008. Fluid and deformation induced partial melting and melt volumes in low-temperature granulite-facies metasediments, Damara Belt, Namibia. *Lithos* **105,** 253–71.

Zinner, E. & Crozaz, C. 1986. A method for the quantitative measurement of rare earth elements in the ion probe. *International Journal of Mass Spectrometry and Ion Processes* **69**, 17–38.

MS received 5 December 2007. Accepted for publication 10 November 2008 (Stellenbosch); 15 January 2009 (RSE).